Amplitude Amplified Dual-Mass Gyroscope: Design Architecture and Noise Mitigation Strategies

Danmeng Wang, Alexandra Efimovskaya, Andrei M. Shkel
MicroSystems Laboratory, Department of Mechanical and Aerospace Engineering
University of California, Irvine, CA 92697, USA
Email: {*danmenw, aefimovs, ashkel*}@uci.edu

***Abstract*—This paper presents our latest test results of an amplitude amplified dual-mass MEMS gyroscope. We discuss the effects of quadrature errors, parasitic capacitance, and front-end components on gyroscope's performance. Three mitigation strategies were utilized, including (1) precision electrostatic frequency tuning to reduce quadrature errors and to compensate for imperfections; (2) increased sensing capacitance to boost Signal-to-Noise Ratio (SNR); (3) a custom low-noise front-end electronics with balanced and differential pick-off channels to improve SNR and reduce noise. A performance of 0.09 deg/hr in-run bias stability and 0.0096 deg/rt-hr Angle Random Walk (ARW) were reported in the paper.**

Keywords: MEMS gyroscopes; amplitude amplification; dual-mass gyroscope; electrostatic tuning; quadrature errors

I. Introduction

Essential attributes of high precision Coriolis Vibratory Gyroscopes include high Quality factor (Q-factor), isotropic stiffness, symmetric damping, and low noise interference. To achieve these objectives, a variety of multi-mass solutions emerged to design a different gyroscope architecture, each offering their own advantages. For example, the Dual Foucault Pendulum (DFP) gyroscope has an ability to dynamically balance reaction forces and moments applied to the anchor for both operational modes, thus increasing the Q-factor to over 1M [1]. A different type of solution to improve performance is to utilize an amplitude amplified dual-mass gyroscope, which offers an increased amplitude of response leading to an increased SNR [2], [3]. In addition, it is also imperative to reduce noise sources and increase the SNR of the sensor. Generally, there are three main approaches to achieve a higher SNR: remove the source of noise, reduce the effect of noise, and increase the measured signal.

In this paper, we utilized an inherent advantage of the dual-mass amplitude amplified gyroscope to increase the SNR. In addition, we employed several mitigation strategies for reducing the noise, including the compensations of quadrature errors, parasitic capacitance, and effects of unbalanced front-end electronics.

This material is based on work supported by the Defense Advanced Research Projects Agency and U.S. Navy under contract No. N66001-16-1-4021.

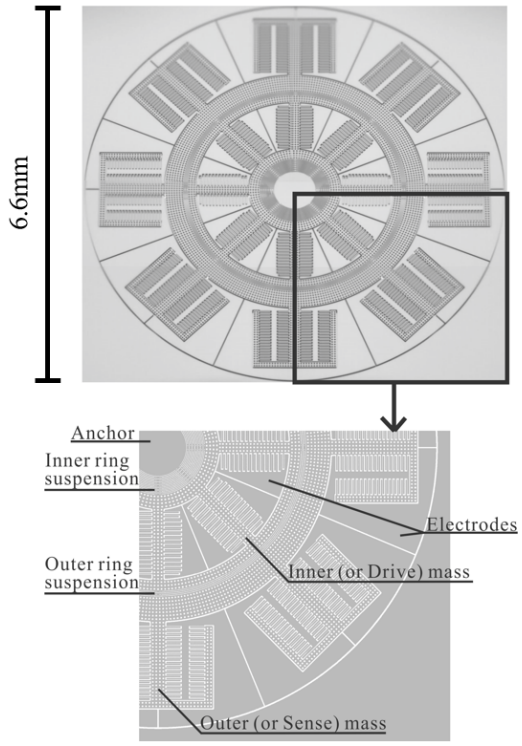

Fig. 1. A prototype of the dual-mass gyroscope and a close-up of a quarter of the device showing the central anchor, concentric ring suspensions, and electrodes.

II. Dynamic Amplification

A. Dual-mass Structure

We report our progress in development of amplitude amplified dual-mass gyroscope, illustrated in Fig.1. The device includes an inner mass, or the drive mass, attached to a central anchor, and an outer mass, or the sense mass, attached to the drive mass using a concentric ring suspension. The device has a footprint of 6.6x6.6 mm^2 and was fabricated using an in-house SOI fabrication process, utilizing a 50 μm-thick silicon device layer, a 500 μm handle wafer, and a 5 μm-thick buried oxide layer between the handle and the device layer.

B. Amplitude Amplification

The dual-mass structure utilizes an increased number of degrees of freedom, from 2-DOF to 4-DOF, to achieve the amplitude amplification between the drive (inner) mass and

978-1-5386-7828-2/19/$31.00 ©2019 IEEE

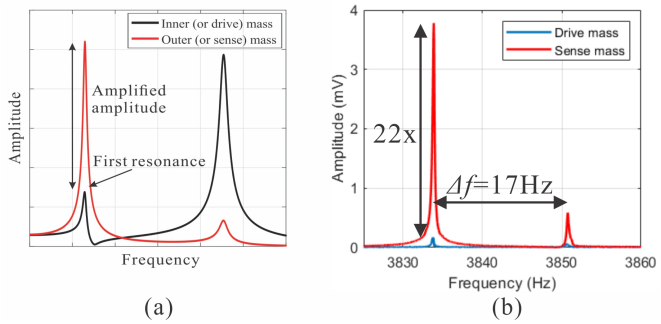

Fig. 2. (a) Frequency response of a dual-mass architecture with amplitude amplification. (b) By electrostatically actuating the drive mass at the first resonance, a 22x signal amplification is achieved.

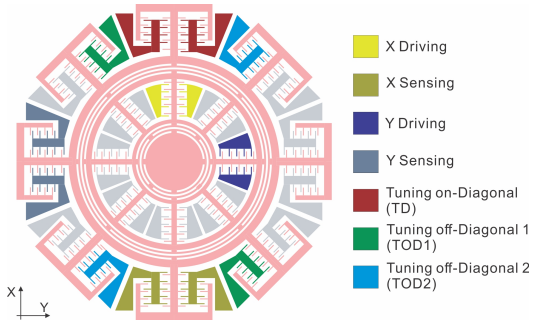

Fig. 3. Configuration of driving, sensing, and tuning electrodes of amplitude amplified dual-mass gyroscope.

the sense (outer) mass. The equations of motion are derived using a dual mass-spring-damper model along the drive axes (x_1 and x_2) and the sense axes (y_1 and y_2) [2]:

$$\ddot{x}_1 + \frac{c_1}{m_1}\dot{x}_1 + \frac{k_1+k_2}{m_1}x_1 - \frac{k_2}{m_1}x_2 = \frac{F_x}{m_1} + 2\Omega\dot{y}_1 \quad (1)$$

$$\ddot{x}_2 + \frac{c_2}{m_2}\dot{x}_2 + \frac{k_2}{m_2}x_2 = \frac{k_2}{m_2}x_1 + 2\Omega\dot{y}_2 \quad (2)$$

$$\ddot{y}_1 + \frac{c_1}{m_1}\dot{y}_1 + \frac{k_1+k_2}{m_1}y_1 - \frac{k_2}{m_1}y_2 = \frac{F_y}{m_1} - 2\Omega\dot{x}_1 \quad (3)$$

$$\ddot{y}_2 + \frac{c_2}{m_2}\dot{y}_2 + \frac{k_2}{m_2}y_2 = \frac{k_2}{m_2}y_1 - 2\Omega\dot{x}_2 \quad (4)$$

In Equations (1-4), m_1 and m_2 represent the inner and outer masses, k_1 and k_2 are stiffnesses of the inner and outer ring suspension, and c_1 and c_2 are damping coefficients associated with each mass. Parameters x_1 and y_1 are displacements of the inner mass (or drive mass) and x_2 and y_2 are displacements of the outer mass (or sense mass) along the x- and y-axis. Ω is a constant input angular rotation along the z-axis, and F_x and F_y are the sinusoidal driving forces applied to the inner mass along the x- and y-axis. The frequency of the driving force is the first resonant frequency of the coupled dual-mass system, Fig.2(a), where the dynamic amplification condition is satisfied.

Due to a mechanically amplified amplitude of the sense mass, the dual-mass architecture possesses larger amplitude of response, smaller (more linear) amplitude of actuation, and higher sensitivity. We designed the reported device with 11.5 amplitude amplification and the experimental result is shown in Fig.2(b). The y-axis in the figure is the output electrical signals of both drive and sense masses, measuring a 22x amplitude difference. Since the capacitance in sense mass is 2x larger than the capacitance in drive mass, the displacements of each mass were obtained after compensating the 2x capacitance differences between the masses, resulting in the measured amplitude amplification factor (AF) 11x (half of the actual 22x amplitude amplification).

III. NOISE SOURCES AND MITIGATION STRATEGIES

Noises in MEMS gyroscopes have intrinsic and extrinsic origins. The main internal noise in bulk micro-machined gyroscopes with capacitance detection include mechanical-thermal noise (MTN), electronic thermal noise (ETN), flicker noise (FN), quadrature error (details discussed in [4]), and parasitic capacitance. MTN and ETN are functions of temperature. FN is a function of frequency of a feed-through signal from the drive to the sense port. The external noise signals coupled to MEMS gyroscopes are diverse and they vary with temperature, ambient vibration, and pressure within the package. Precision thermal control and vacuum packaging reduce the external noise sources. A well-designed and balanced front-end circuit with low-noise components helps to reduce the electronic noise.

The focus of this paper is to explore how the compensations of quadrature errors, parasitic capacitance, and unbalanced front-end electronics affect performance of the amplitude amplified dual-mass gyroscope.

A. *Quadrature Errors*

Unbalance suspension springs due to fabrication imperfections is a dominant source of quadrature errors, [5], resulting in a frequency split between operational modes and misalignment of the principal axes of elasticity. The amplitude amplified architecture has a dual-spring suspension system, which is intrinsically difficult to compensate for quadrature errors due to an increased degree of freedom of the system from two to four. In this study, we implemented a precision electrostatic frequency tuning method for our dual-mass gyroscope, reported in [6], which involved an off-diagonal tuning to decouple the operational modes and a on-diagonal tuning to electrostatically softening of the stiffer mode.

The amplitude amplified dual-mass gyroscope reported in this paper had an as-fabricated frequency split (Δf) of 17 Hz. To mitigate the frequency split, an electrostatic compensation was applied along the x-axis, Fig.3. A DC voltage difference of 7.4 V between TOD1 and TOD2 electrodes was first applied for off-diagonal tuning, followed by a DC voltage of 13.5 V applied on TD electrodes for on-diagonal tuning. The frequency mismatch was electrostatically tuned down to 0.5 Hz, Fig.4, and the gyroscope′s scale factor improved by 14x, from 0.7 to 9.7 mV/deg/s, Fig.5, due to reduced coupling between operational modes and minimizing the quadrature errors.

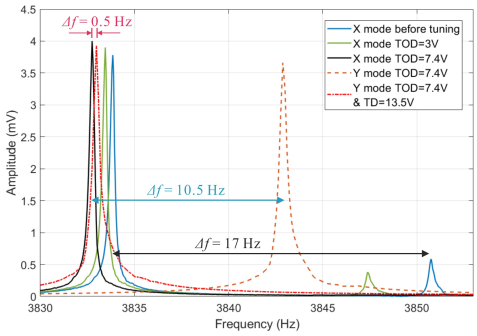

Fig. 4. Frequency response showing an off-diagonal tuning of stiffness, minimizing the coupling between modes (Δf reduced from 17 to 10.5 Hz), and the on-diagonal tuning of the stiffness, reducing the frequency mismatch to 0.5 Hz.

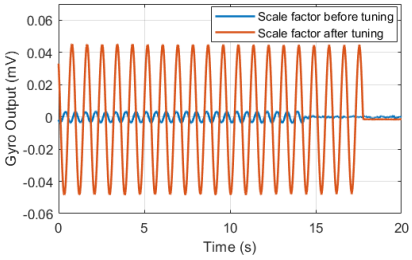

Fig. 5. Gyroscope response on a rate table due to a sinusoidal input of rotation at the rate of 5 deg/s, showing a 14x higher scale factor and an increased stability of the response amplitude after tuning.

B. Parasitic Capacitance

Parasitic capacitance in MEMS devices is inevitable and is often on the order of the sense capacitance. The feedthrough current created by the parasitic capacitance between the drive and sense electrodes is one of the main noise sources. In this study, we assumed that the feedthrough parasitic circuit consists of a single lumped capacitor, C_p. Equations of total output current measured by sense electrodes, [7], and SNR are as follows:

$$I(t) = C_s V_c F_1(\omega_d, \omega_c, t) + C_p V_d F_2(\omega_d, t) \quad (5)$$

$$SNR = C_s V_c F_1(\omega_d, \omega_c, t) / C_p V_d F_2(\omega_d, t) \quad (6)$$

Both equation contain two terms: (1) the sensing current (signal term), which is a function of the sensing capacitance, C_s, the carrier signal, V_c, and the driving and carrier frequency, ω_d and ω_c; (2) the feedthrough current (noise term), which is a function of the parasitic capacitance, C_p, and the driving signal, V_d.

From Equation (6) of SNR, an increased sensing capacitance, C_s, or carrier signal, V_c, would increase the SNR. We maximized the sense capacitance in our design of the dual-mass gyroscope, achieving 8 pF. However, the carrier signal has a limitation caused by the testing instrument, which will be discussed in the following section.

C. Front-End Circuit

Zurich Instrument lock-in amplifier (HF2LI) was employed in characterization of the dual-mass amplitude amplified gyroscope. Due to 2 V_{pp} limitation of the input signals of HF2LI,

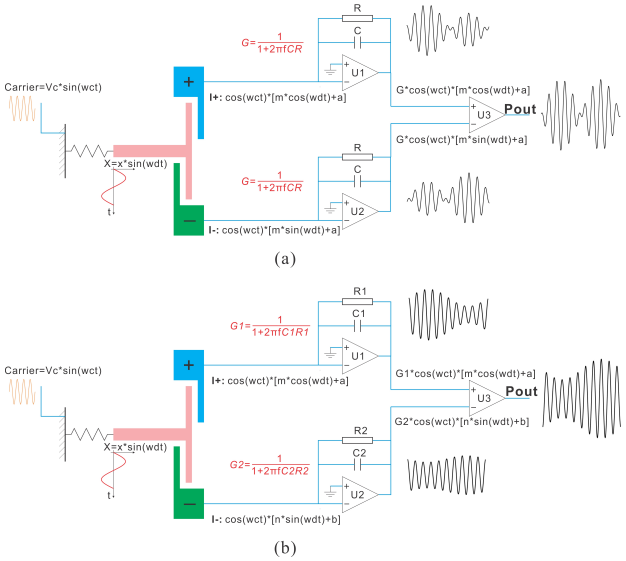

Fig. 6. Schematics of a simplified control electronics of differential detection for (a) an ideal case (a carrier signal term cancelled) and (b) an unbalanced case (a large carrier signal term remained).

the carrier signal applied to the proof-mass was also limited. Ideally, a differential detection, Fig.6(a), can effectively reduce the noise and the carrier signal term before signals enter HF2LI. However, in reality, the differential signals obtained by differential electrodes, i_+ and i_-, will be amplified several million times by two separate amplifiers (U_1 and U_2) of the front-end circuit, which always contains unequal gains, G_1 and G_2, Fig.6(b). The values are then subtracted by another amplifier (U_3). In this paper, we refer to the sequence of processes as unbalanced sensing paths. Because of the unbalance in the sensing paths, a significant carrier signal term remained in the final sensing signal. In previous studies, the residual gains error was up to 12%, limiting the carrier signal to 1 V_{pp} AC at 52 kHz in our tests.

To effectively remove the carrier signal term from the final sense signal before entering HF2LI, a differential detection with balanced sensing paths in the front-end electronics was designed, Fig.7. The balanced sense paths were achieved by matching the amplification gain (by matching the corresponding resistors and capacitors) in each differential amplifier of the circuit. This allowed a 52 kHz AC signal as large as 10 V_{pp} to be applied to the proof-mass of the gyroscope as the carrier signal. The sensitivity of the device improved by 3.67x while the carrier signal increased from 1 to 10 V_{pp} AC, Fig.8.

The front-end electronics also contained low-noise amplifiers and low-noise power regulators with the noise level of 131 nV/rt-Hz and 6M amplification, to reduce the noise contaminating the sensing signals.

IV. CHARACTERIZATION

The amplitude amplified dual-mass gyroscope was characterized in a vacuum chamber on the rate table (Ideal Aerosmith 2102). To remove external vibratory noise of continuous pumping of the vacuum chamber and to reduce the thermal noise effect, we employed a vacuum chamber

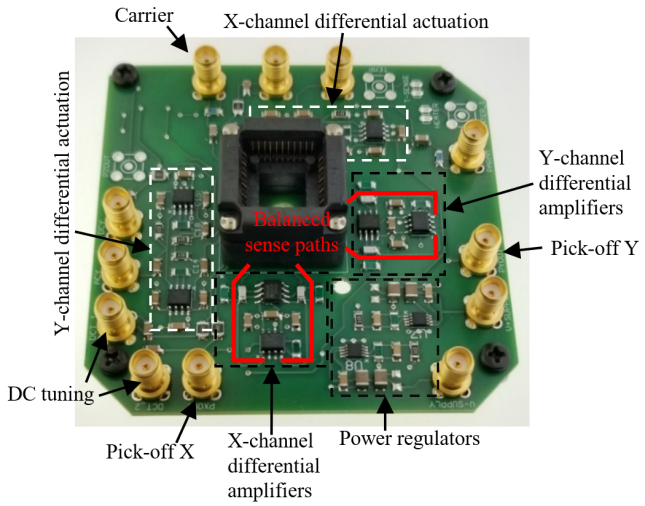

Fig. 7. The balanced low-noise front-end circuit with 2-channel differential drive and 2-channel differential pick-off.

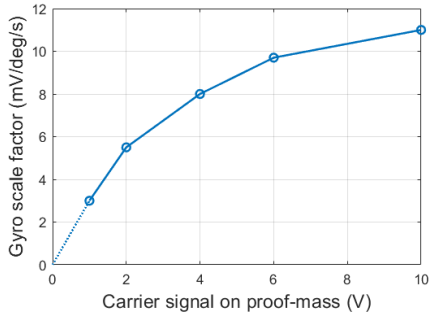

Fig. 8. Gyroscope response with different carrier signal amplitudes from 1 to 10 V_{pp} (52 kHz), revealing an improvement of the open-loop scale factor from 3 to 11 mV/(deg/s).

connected to a vibration-free pump (SPCe Ion pump) for >7 days steady period under lab temperature to achieve an ultra-high vacuum level (3e-8 Torr) with stabilized vacuum and temperature (<1e-9 Torr and <0.5 deg fluctuation for 10 hours of recording). Phase-Locked Loop and Amplitude Gain Control were utilized in the control loop with details of the design parameters and experimental results summarized in Table I. The frequency split was electrostatically tuned down to 0.5 Hz and 6 V_{pp} AC signal carrier was applied to the proof-mass. The scale factor extracted was 9.7 mV/deg/s.

Utilizing advantages of the dual-mass structure and discussed noise reduction strategies, 0.09 deg/hr in bias stability and 0.0096 deg/rt-hr in ARW were experimentally demonstrated for the open-loop angular rate mode of operation, Fig.9.

V. Conclusion

Dual-mass dynamically amplitude amplified gyroscope with advantages of linearity and increased SNR was studied in this work. The main noise sources, quadrature errors, parasitic capacitance, and unbalanced front-end components were identified as the primary discount factors to performance. We

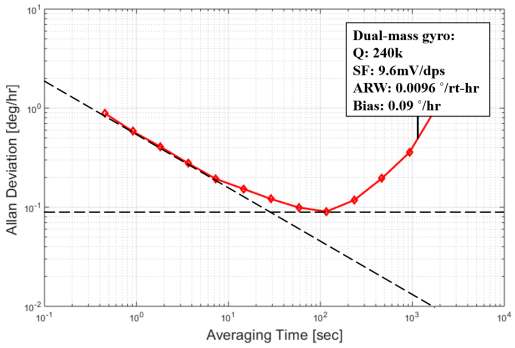

Fig. 9. The Allan Deviation of the amplitude amplified dual-mass gyroscope (tested in a vacuum chamber) in the open-loop operational mode.

TABLE I
DESIGN PARAMETERS AND EXPERIMENTAL RESULTS

	Operational frequency	***Diameter***	C_{drive}	C_{sense}	AF (measured)
Dual-mass gyro	4.3 kHz	6.6 mm	4 pF	8 pF	11x
	As-fab. Δf	Electrostatic tuned Δf	Q_{TED}	Q(measured)	Scale factor
	17 Hz	0.5 Hz	600k	240k	9.7 mV/dps

proposed and implemented the mitigation strategies, which led to improvements in SNR and a reduction of noise. A 0.09 deg/hr in in-run bias stability and a 0.0096 deg/rt-hr ARW in the open-loop rate operation mode were demonstrated, after we electrostatically compensated the frequency mismatch down to 0.5 Hz, leading to 9.7 mV/deg/s scale factor of the gyroscope.

Acknowledgment

The MEMS gyroscopes were designed and characterized at UCI Microsystems Laboratory. Devices were fabricated at UCI INRF cleanroom facility.

References

[1] M. H. Asadian, S. Askari, Y. Wang, and A. Shkel, "Characterization of energy dissipation mechanisms in dual foucault pendulum gyroscopes," in *IEEE International Symposium on Inertial Sensors and Systems (INERTIAL)*, Naples, FL, April 2019.

[2] C. C. Painter and A. M. Shkel, "Dynamically amplified rate integrating gyroscope," Aug. 16 2005, US Patent 6,928,874.

[3] D. Wang, M. H. Asadian, A. Efimovskaya, and A. M. Shkel, "A comparative study of conventional single-mass and amplitude amplified dual-mass MEMS Vibratory Gyroscopes," in *IEEE International Symposium on Inertial Sensors and Systems (INERTIAL)*. IEEE, Kauai. HI, USA, March 27-30 2017.

[4] H. Cao, H. Li, J. Liu, Y. Shi, J. Tang, and C. Shen, "An improved interface and noise analysis of a turning fork microgyroscope structure," *Mechanical Systems and Signal Processing*, vol. 70, pp. 1209–1220, 2016.

[5] E. Tatar, S. E. Alper, and T. Akin, "Quadrature-error compensation and corresponding effects on the performance of fully decoupled mems gyroscopes," *IEEE Journal of Microelectromechanical Systems*, vol. 21, no. 3, pp. 656–667, 2012.

[6] A. Efimovskaya, D. Wang, Y.-W. Lin, and A. M. Shkel, "Electrostatic compensation of structural imperfections in dynamically amplified dual-mass gyroscope," *Sensors and Actuators A: Physical*, vol. 275, pp. 99–108, 2018.

[7] A. A. Trusov and A. M. Shkel, "A novel capacitive detection scheme with inherent self-calibration," *IEEE Journal of Microelectromechanical Systems*, vol. 16, no. 6, pp. 1324–1333, 2007.